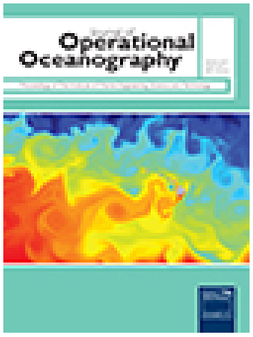

Journal of Operational Oceanography

ISSN: 1755-876X (Print) 1755-8778 (Online) Journal homepage: http://www.tandfonline.com/loi/tjoo20

Comparison between nested grids and unstructured grids for a high-resolution wave forecasting system in the western Mediterranean sea

Elena Pallares, Jaime Lopez, Manuel Espino & Agustín Sánchez-Arcilla

To cite this article: Elena Pallares, Jaime Lopez, Manuel Espino & Agustín Sánchez-Arcilla (2016): Comparison between nested grids and unstructured grids for a high-resolution wave forecasting system in the western Mediterranean sea, Journal of Operational Oceanography, DOI: 10.1080/1755876X.2016.1260389

To link to this article: http://dx.doi.org/10.1080/1755876X.2016.1260389

Published online: 25 Nov 2016.

JOURNAL OF OPERATIONAL OCEANOGRAPHY, 2016
http://dx.doi.org/10.1080/1755876X.2016.1260389

Taylor & Francis
Taylor & Francis Group

Comparison between nested grids and unstructured grids for a high-resolution wave forecasting system in the western Mediterranean sea

Elena Pallares, Jaime Lopez, Manuel Espino and Agustín Sánchez-Arcilla

Laboratori d'Enginyeria Marítima (LIM/UPC), Polytechnic University of Catalonia (UPC), Barcelona, Spain

ABSTRACT

Traditionally wave modelling uses a downscaling process by means of successive nested grids to obtain high-resolution wave fields near the coast. This supposes an uncertain error due to internal boundary conditions and a long computational time. Unstructured grids avoid multiple meshes and thus the problem of internal boundary conditions. In the present study high-resolution wave simulations are analysed for a full year where high-resolution meteorological models were available in the Catalan coast. This coastal case presents sharp gradients in bathymetry and orography and therefore correspondingly sharp variations in the wind and wave fields. Simulations with SWAN v.4091A using a traditional nested sequence and a regional unstructured grid have been compared. Also a local unstructured grid nested in an operational forecast system is included in the analysis. The obtained simulations are compared to wave observations from buoys near the coast; almost no differences are found between the unstructured grids and the regular grids. Simultaneously, tests have been carried out in order to analyse the computational time required for each of the alternatives, showing a decrease to less than half the time when working with regional unstructured grids and maintaining the forecast accuracy and coastal resolution with respect to the downscaling system.

ARTICLE HISTORY
Received 11 February 2016
Accepted 4 November 2016

1. Introduction

A significant part of the European Mediterranean coast is limited in its ability to deal with environmental, physical and hydro-meteorological hazards due to the inhabitation of the first few hundred metres inland. This inhabitation has progressed in most of the locations, on the assumption of a stable coastal fringe. This idea is probably reinforced by a gentle sea state during most of the year, resulting in a false perception of security by society. However, energetic storm events are not rare at all and, when combined together with high water levels, can cause significant damages. In the last 20 years, extreme storm events have been responsible for at least 50 casualties on the north-western Mediterranean coast and for significant damages in coastal defences, harbours and infrastructure, amounting to over EUR 30 million (Gracia et al. 2014).

The Catalan coast is not an exception. Located in the northeast corner of Spain, on the north-western Mediterranean Sea, Catalonia is a Spanish region that in 2014 received 16.8 million tourists, who spent around EUR 15,000 million. The harbour facilities together with the touristic attractions of Barcelona city, the nice weather and its strategic location on the Western Mediterranean Sea and in Europe have been the main reasons for several cruise companies picking Barcelona as their main port of call. But tourism is not the only activity affecting the coastal areas in Catalonia. On the one hand, there are several economical activities affected by the ocean conditions, such as maritime transport or fisheries. On the other hand, along the Catalan coast it is easy to find promenades, buildings, roads and even railways very close to the coast that are highly exposed to the meteo-oceanographic conditions.

Thanks to advances in numerical tools and coastal observations it is now possible to implement operational high-resolution forecast models (waves, oceanic and sediment transport) yielding timely and valuable intervention data to reduce coastal risks due to incoming storms. In the framework of these ideas, the European Union has supported the iCoast project (www.icoast.eu) in order to develop a methodology to set up an early warning system to minimise the coastal hazards due to storm events on European coasts. The present study is part of the wave forecasting system proposed in the framework of the project applied to the Catalan coast, where the SWAN model v.40.91A (Booij et al. 1999; Ris et al. 1999) has been used to provide

CONTACT Elena Pallares elena.pallares@upc.edu Laboratori d'Enginyeria Marítima (LIM/UPC), Polytechnic University of Catalonia (UPC), Jordi Girona, 1-3, Ed. D1, 08034 Barcelona, Spain

high-resolution wave conditions in a reduced time frame. This reduction of time is decisive in the period previous to a storm event, when certain decisions need to be made in order to minimise the impacts in coastal areas.

Although nowadays there are several operational systems providing wave forecasts in the study area, all of them use the traditional methodology of nested grids to improve the resolution in some coastal areas. In the present study different grid configurations are tested, including unstructured grids as an alternative to the downscaling process, and considering the use of boundary conditions from an external system, in order to obtain high-resolution wave forecast that are as accurate as possible while reducing the computational time.

The paper is structured in three main sections. First, a detailed revision of the methodology is presented, including an introduction of the study area, a brief description of the Simulating Waves Nearshore (SWAN) wave model, a revision of the usage of unstructured grids in wave modelling, followed by the experiment configuration, the data available and the computer characteristics. Next are presented part of the results obtained during the development of the study for a one-year period and during a storm event. The paper finishes with a discussion section and the conclusions.

2. Methodology

2.1 Study area

The wave forecast presented in this study is focused on the Catalan coast, despite all the configurations covering the Western Mediterranean Sea. The Catalan coast is located on the north-eastern Spanish coast, between latitudes 40°45′N and 42°25′N and longitudes 0°45′E and 3°15′E, and has a length of about 600 km. The Pyrenees mountain range, located northern of the study domain, is the main orographic feature in the area and determines in great measure the meteorological conditions on the coast. The wind fields are highly variable, mainly controlled by the heterogeneous orography, the air–sea temperature differences and the passage of low-pressure centres from the Atlantic. The prevalent winds, on average not very intense except for storm events, come from the north and north-west, mainly during winter; southerly and easterly winds are also important, particularly during the months of February, March, April and November (Arnau 2000). When the wind blows from the north, the mountain ranges induce wind channelling through river valleys, with the most important being the Ebro Delta wind jet. These characteristic land-to-sea winds are highly variable both in space and time (Sánchez-Arcilla et al. 2008) and are particularly intense and persistent during autumn and winter (Alomar et al. 2014).

The predominant wave direction, as happens with the wind fields, varies along the coast, showing the topographic control due to a complex bathymetry, with submarine canyons and a heterogeneous continental shelf width (Sánchez-Arcilla et al. 2008; Bolaños et al. 2009). Sánchez-Arcilla et al. (2008) describe how the southern and northern sections of the coast show a predominance of north-west and north wave conditions, while the central part of the Catalan coast is dominated by east and south wave conditions. The higher waves come from the east, where the largest fetches and stronger winds coincide. In the areas where the wind blows from the north-west (offshore winds), there is a tendency to develop a large amount of bimodal spectra due to the co-existence of sea and swell waves (Bolaños et al. 2007).

2.2 The SWAN model

The SWAN Cycle III v.4091A code has been used to simulate the wave evolution in the area. SWAN is a third-generation wave model that computes random, short-crested wind generated waves in coastal regions and inland waters (Booij et al. 1999; Ris et al. 1999). This model is an extension of deep water third-generation wave models based on the wave action balance equation with sources and sinks: it incorporates the triad wave–wave interactions and the depth-induced breaking, which are especially useful in shallow waters; it also admits ambient currents as an input.

Pallares et al. (2014) performed a calibration process of the SWAN model for semi-enclosed domains, particularly on the Catalan coast; the coefficients determined therein have been used in the present work. Spherical coordinates and nautical convention have been selected. The wind growth is obtained as the sum of a linear term due to Cavaleri and Malanotte-Rizzoli (1981) and an exponential term that is the same one used by WAM Cycle 3, due to Snyder et al. (1981) and rescaled by Komen et al. (1984). The quadruplet non-linear wave–wave interactions are computed using the Discrete Interaction Approximation proposed by Hasselmann et al. (1985). The whitecapping term used is the Komen et al. (1984) formulation but using a delta coefficient of 1. Regarding the numerical aspects, the scheme for geographic propagation has a maximum number of iterations per time step of 15, and a time step of 15 min has been chosen, which is small enough to reproduce the wind and wave variability but still allows an affordable computational cost. The frequency range considered

is 0.01–1 Hz, with 49 values logarithmically spaced with a frequency resolution of $df/f = 0{,}1$ as recommended by the SWAN manual (SWAN team 2015a), and the directional resolution is 10°.

2.3 Unstructured grids

Traditionally, the methodology to improve the resolution of wave forecasting near the coast consists of a downscaling process with a system of nested domains, each with a smaller resolution and covering a smaller area than the previous one (Alari et al. 2008; Alomar et al. 2014; Sánchez-Arcilla et al. 2014), where the required boundary conditions are provided by the coarser mesh.

In the present study the usage of an unstructured grid with a varying mesh size is also considered. The main advantage of using an unstructured grid for wave modelling is that it allows working with a single grid with different resolutions at each sub-domain, thus improving the resolution in coastal areas, and therefore the nesting is not needed. Another advantage is that the unstructured grid is able to reproduce the sharp coastline more accurately than regular meshes. Finally, unstructured grids allow indirectly what is known as two-way nesting, where information is transferred not only from the coarser to the finer domain but also in the other direction – a process especially interesting in situations with inland winds, such as the case of the Mistral on the Mediterranean coast.

The unstructured grids have been used in wave modelling mainly in small domains (Hsu et al. 2005; Zijlema 2010; Siadatmousavi et al. 2015) nested to regional or global grids. This more typical approach is presented in the present study in comparison to a regional unstructured grid designed to cover the entire Western Mediterranean Sea.

The SWAN model is able to work with both types of grids, nested regular systems and unstructured grids, using exactly the same physics, allowing a comparison under the same conditions. Zijlema (2010) presents and validates the numerical scheme adapted for unstructured grids, consisting of a vertex-based, fully implicit, finite-differences method that requires several sweeps through the grid. For the regular grids, SWAN provides several numerical schemes; however, among them the one that was used for this exercise is the backward space and backward time, a first-order upwind scheme (SWAN team 2015b), since it is the equivalent to the numerical scheme used for the unstructured grids. As mentioned by Zijlema (2010), in most of the situations the CPU cost per grid point is higher for the unstructured meshes; however, the reduction of the number of grid points in this type of meshes offsets the total time.

2.4 Experimental configuration

Four different configurations have been tested to determine which may be the best option, regarding the accuracy of results and the computational time, when designing an operational wave forecasting system (Figure 1). Different situations are considered: on the one hand, the regular nested grids are compared with a unique unstructured mesh, while, on the other hand, the systems covering the entire Western Mediterranean Sea, a semi-enclosed domain, are compared with local grids nested in actually running regional forecast systems. The aim of this comparison is to provide accurate wave conditions with high resolution in coastal areas in an efficient way.

Regarding the grids covering the entire semi-enclosed domain, the regular nested system (herein named A) is comprised of three meshes with a spatial resolution of 9, 3 and 1 km, while the regional unstructured mesh for the Western Mediterranean Sea (herein named B) has 8317 elements and 4548 nodes, with a resolution from 40 km in open waters to 800 m in shallow waters (Figure 2(a)). Similar systems to the ones presented previously are considered in the second alternative, albeit covering a smaller area, the Balear Sea, and nested to an actually running regional operational system. The first one (herein named C) consists of the two smaller regular nested grids (with 3 km and 1 km spatial resolution), and the second one consists of a local unstructured grid covering the same area (herein named D), with 4928 elements and 2710 nodes, with a resolution from 25 km at the boundaries to 800 m in the coastal area (Figure 2(b)). In Tables 1 and 2 the characteristics of all the meshes used and the configurations considered are presented.

In order to provide some general results and conclusions, avoiding the seasonal effects, one year of simulations is performed, corresponding to 2013. Additionally, a storm event is also analysed in detail, since during these periods the information provided by the model forecast needs to be more accurate, mainly for coastal early warning systems as mentioned previously.

2.5 Data available

Three buoys located along the Catalan coast and operated by the Spanish harbour agency Puertos del Estado (www.puertos.es) were considered for the validation

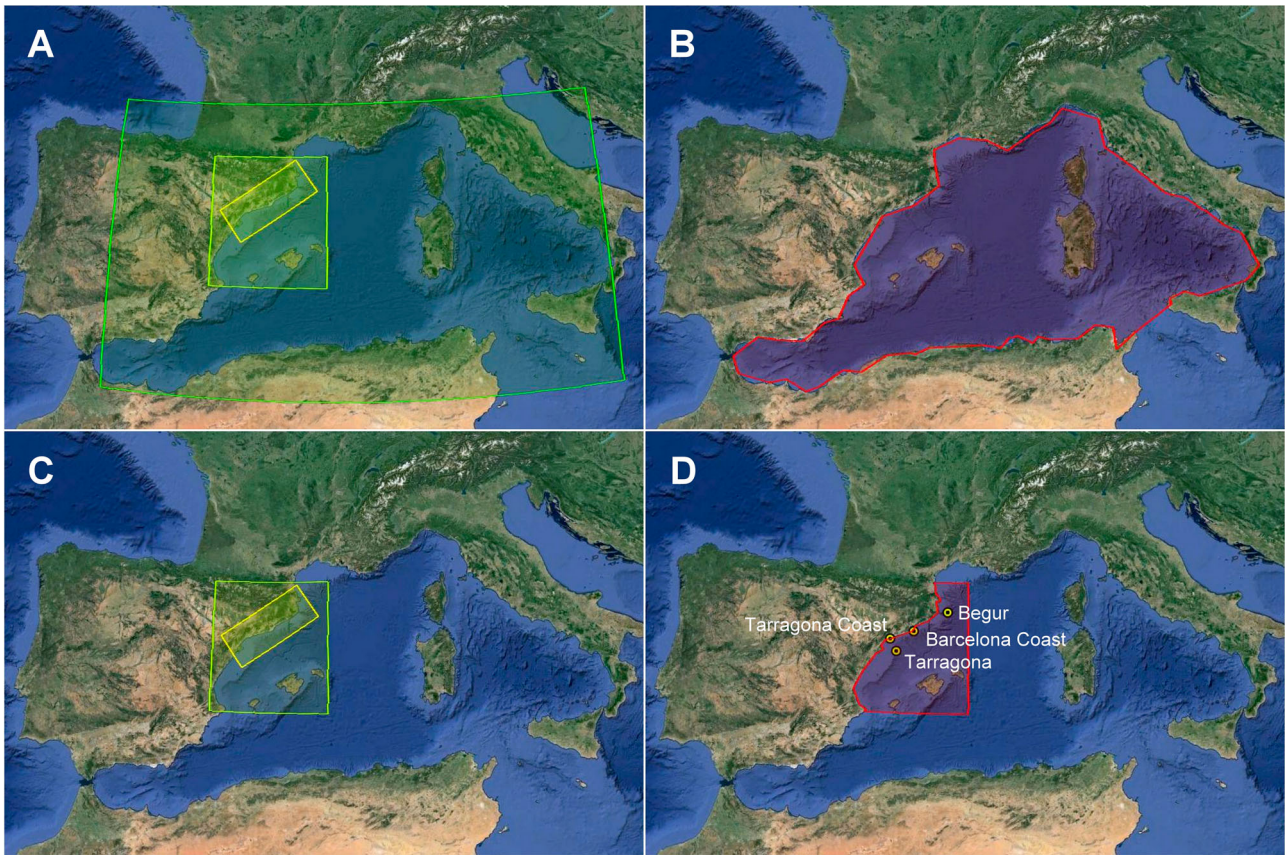

Figure 1. Representation of the four configurations tested in the study. The small circles in configuration D represent the buoy locations. Source: Google, Landsat.

process. Two of the buoys, Barcelona coast and Tarragona coast, are moored near the coast; the other buoy, Tarragona, is moored in deep waters (Figure 1, Table 3). The bathymetry used for the simulations is obtained from GEBCO (General Bathymetric Chart of the Oceans, www.gebco.net) with a grid resolution of 30 arc-seconds (.0083°, around 900 m in these latitudes).

The winds for the present study have been provided by the Spanish Meteorological Agency (AEMet, www.aemet.es) and include a coarser wind field that provides the wind conditions 10 m above the sea level, with a spatial resolution of .16° (around 16 km in these latitudes) for the entire Western Mediterranean Sea, and a better resolution wind field that covers only the Catalan coast area, with a spatial resolution of .05° (around 5 km in these latitudes). Both wind fields are obtained using the High Resolution Limited Area Model (HIRLAM) (Unden et al. 2002) and have a temporal resolution of 1 h and a forecast horizon of 72 h. In the present study analysed winds have been used for the two resolutions available, herein named HIRLAM .16° and HIRLAM .05°.

The bad accuracy of the winds, especially when the resolution is low, is commonly reported as one of the main causes of poor results of the wave models near the coast (Ardhuin et al. 2007), so a validation of the wind fields over the sea has been performed for a one-year period. Since it has not been possible to find other wind measurements on the sea for the selected period, only one validation location is presented, corresponding to the Tarragona buoy described previously.

The results obtained are shown in Figure 3, where the empirical histograms obtained as the distribution of the different winds during the whole period are presented using a range of 1 m/s. Additionally, some statistics (detailed in Section 3.1) have been calculated and are shown in Table 4. From the validation process it can be stated that the general quality of the wind is acceptable, with correlation coefficients around .85 in intensity and slightly lowers, around .67, in direction for the two models. However, both of them tend to underestimate the wind lower than 2 m/s, and overestimate the intensity of the wind fields for higher velocities (2–6 m/s). For winds over 10 m/s (important during storm events), both models present a similar slightly overestimation. On the other hand, the root mean square error (RMSE) of the direction obtained for both wind fields are a little bit high due to the highly variability in wind and wave directions in the measurement location. In conclusion, in the validation location there are no

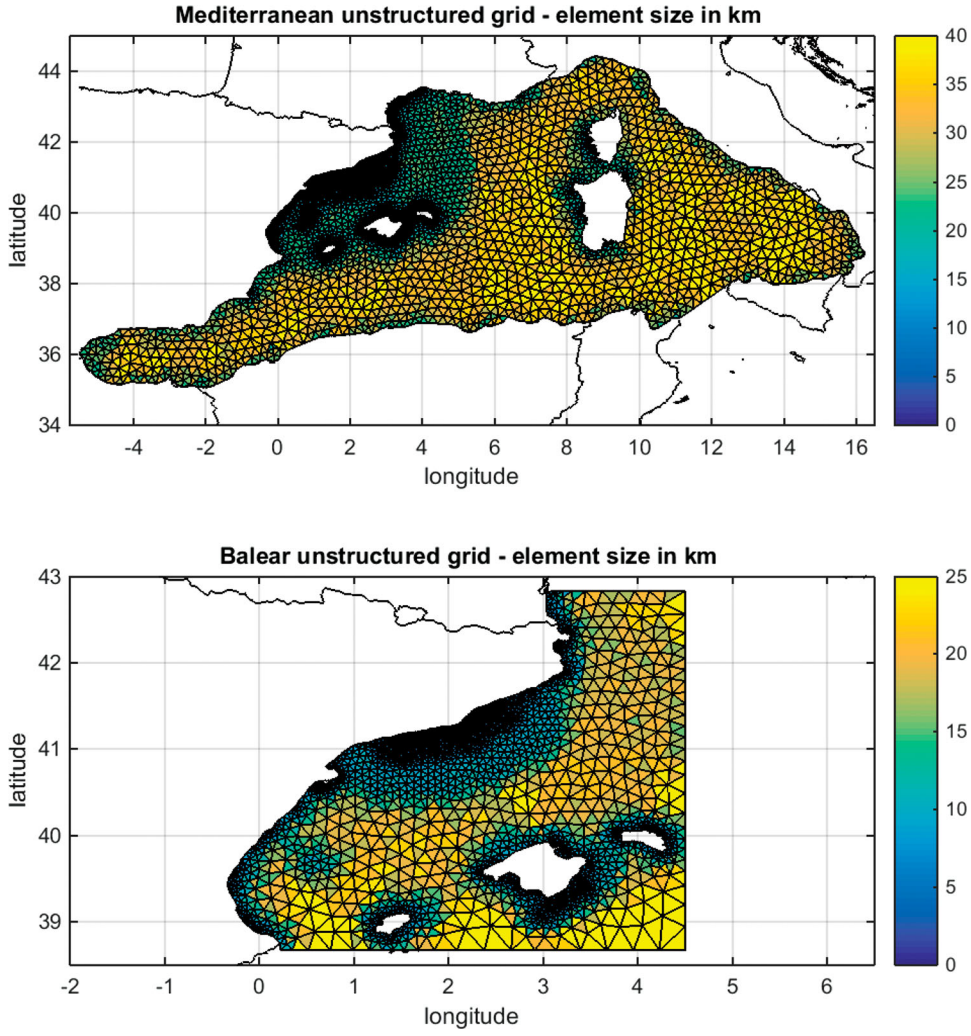

Figure 2. Detail of the unstructured grids used for the western Mediterranean sea grid (top), used as configuration B, and the Balear unstructured grid (bottom), used in configuration D. The colour scale represents the grid size in km as the medium length of the sides of each triangle.

Table 1. Description of the grids used in the study, including the mesh resolution, the domain covered, the number of grid points for regular grids and the number of nodes and triangles for unstructured grids and the wind forcing.

Grid	Resolution	Lat–Lon	Grid points	Wind forcing
Mediterranean regular	9 km	4.900 W–16.048 E 35.000 N–44.523 N	119 × 196 (23,324 nodes)	HIRLAM .16°
Balear regular	3 km	0.470 W–4.500 E 38.670 N–42.830 N	155 × 139 (21,545 nodes)	HIRLAM .16°
Local regular	1 km	0.145 E–3.291 E 40.083 N–42.787 N	136 × 332 (45,152 nodes)	HIRLAM .05°
Mediterranean unstructured	40 km to 800 m	5.495 W–16.218 E 35.091 N–44.424 N	4548 nodes 8,317 triangles	Merged wind
Balear unstructured	25 km to 800 m	0.331 W–4.500 E 38.670 N–42.830 N	2710 nodes 4928 triangles	Merged wind

Table 2. Description of the four configurations considered in the present study, named A–D and formed by one or several grids. The need of boundary conditions is resumed in the third column.

Configuration	Grids used	Boundary conditions
A	Mediterranean regular Balear regular Local regular	No
B	Mediterranean unstructured	No
C	Balear regular Local regular	Yes
D	Balear unstructured	Yes

Table 3. List of the instruments location and the information provided by each of them for the Catalan coast.

Name	Lon	Lat	Depth	Parameters provided
Begur	3.65° E	41.92° N	1200 m	Hs, Dir, Tm_{02}, Tp, Wind
Barcelona coast	2.20° E	41.28° N	68 m	Hs, Dir, Tp
Tarragona	1.47° E	40.68° N	688 m	Hs, Dir, Tm_{02}, Tp, Wind
Tarragona coast	1.19° E	41.07° N	15 m	Hs, Dir, Tp

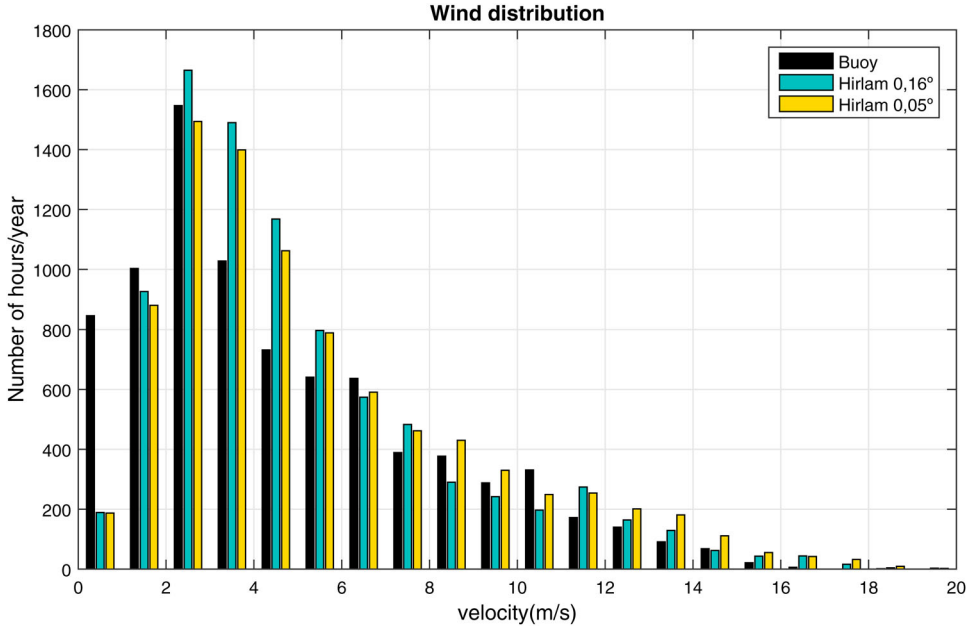

Figure 3. Empirical histogram of the wind intensity (m/s) for the buoy measurements, the HIRLAM .16° wind model and the HIRLAM .05° high-resolution wind model for the 2013.

important differences in the accuracy of the two models despite the different resolution, so one cannot be considered to work better than the other. However, as Alomar et al. (2014) concluded, the wave field tends to improve considerably when forced by winds with better resolution in space and time, so when possible the high-resolution wind field will be used instead of the coarser one. In Table 1 the wind forcing used for each of the SWAN domains is detailed.

For both unstructured grid configurations a unique wind field can be used, so to take advantage of the high-resolution information a merging process has been performed to combine both existing wind fields into a new one. Since both wind fields proceed from the same source and the continuity is assured, the merging process consisted in interpolating the boundaries.

As previously introduced, in order to avoid some computational time when running the coarser wave domain, a consideration has been to nest our system to an actually working operational service. The boundary conditions necessary for running configurations C and D are obtained from the wave forecast system of the Spanish harbour agency, Puertos del Estado, using the significant wave height, the mean wave period, the mean wave direction and the wave spread coefficient to generate a theoretical spectrum at the boundaries. The operational forecast system, described in Gomez and Carretero (2005), consists of an application of the WAM model (the WAMDI group 1988) for the Spanish Mediterranean coast, with two nested domains with a spatial resolution from 5 to 10 min and a temporal resolution of 1 h that are operated on a twice-a-day cycle and provide a forecast horizon of 72 h. However, analysed wave fields have been used in the present study. The system is forced with the HIRLAM .16° wind field described previously.

Table 4. Results of the validation of the two wind models including the wind intensity (m/s) and wind direction (deg) for the 2013 year in Tarragona buoy location.

	Wind intensity				Wind direction		
Model	RMSE [m/s]	Bias [m/s]	SI	*R*	RMSE [°]	SI	*R*
HIRLAM .16°	1.89	.54	.397	.844	77.45	.368	.668
HIRLAM .05°	2.02	.92	.424	.856	77.08	.214	.667

2.6 Computational structure

The computations were performed in a small cluster named 'Alien' belonging to the computational centre of the civil engineering school of Barcelona, BarcelonaTech. The machine is made up of Dell computers and a Red Hat Linux operating system, including four nodes with Intel processors and two nodes with AMD processors. Each of the four Dell PowerEdge R900 nodes has four quad-core Intel Xeon processors with 2.4 GHz, 16 MB of L3 cache per processor and 128 GB of RAM, while the two Dell PowerEdge R805 nodes have quad-core AMD Opteron processors with 2.5 GHZ, 6 MB of cache per processor and 32 GB of RAM.

An initial test was performed to determine the time requirements for running the SWAN model depending

on the number of CPUs used. The Western Mediterranean Sea domain was chosen for the exercise, forced with the HIRLAM .16° wind field, for a period of three days. Only the Intel nodes were considered, and the parallelisation was carried out through the OpenMP protocol.

The results presented in Figure 4 show an exponential decrease of the computational time required to run the model when increasing the CPUs. The reduction of time is especially significant from one to eight processors, while adding more processors does not result in an appreciable time savings. It can be concluded that, for the machine used, the optimal situation would be to work with eight or more processors. However, the machine available is shared with other users, so only one core can be guaranteed per jobs (equivalent to four processors). For this reason it was decided herein to use four processors to run the SWAN model.

3. Results

3.1 Validation tools

The validation of results from the different simulations was mainly based on time series and Taylor diagrams (Taylor 2001). Some statistical parameters have also been also employed for quantitative comparisons; the main ones are the RMSE, the bias, the scatter index (SI) and the correlation coefficient (R). These parameters are obtained as follows:

$$\mathrm{RMSE} = \sqrt{\frac{\sum_{i=1}^{N}(S_i - O_i)^2}{N}}, \tag{1}$$

$$\mathrm{bias} = \frac{\sum_{i=1}^{N}(S_i - O_i)}{N}, \tag{2}$$

$$\mathrm{SI} = \frac{\mathrm{RMSE}}{\bar{O}}, \tag{3}$$

$$R = \frac{\sum_{i=1}^{N}((S_i - \bar{S})\cdot(O_i - \bar{O}))}{\sqrt{\sum_{i=1}^{N}(S_i - \bar{S})^2}\cdot\sqrt{\sum_{i=1}^{N}(O_i - \bar{O})^2}}. \tag{4}$$

where S corresponds to the simulated data and O to the measured ones (observations); N is the number of data; and $\bar{O}$ and $\bar{S}$ correspond to the mean value of the time series for observed and measured values, respectively. All these formulations except the bias have been adapted to analyse the wave direction, considering the minimum angle between the two data (simulated and measured).

The data measured by the instruments and those obtained from the SWAN simulations both correspond to 1 h time resolution for the entire study period, providing a time series longer than 8000 values. The wave parameters considered for the validation are summarised in Table 5. Results from the wave model correspond to the same location as the measurement instruments after an

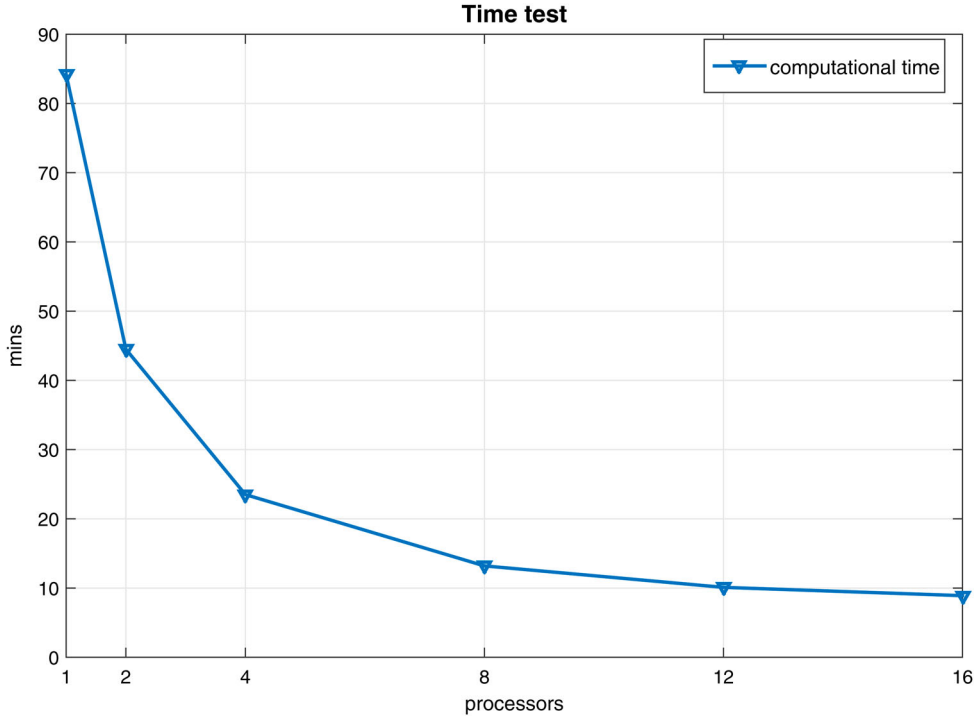

Figure 4. Time requirement in min necessary to run the test case using from 1 up to 16 processors.

Table 5. Definition of the bulk parameters used to compare the SWAN simulations.

Moment	m_n	$m_n = \int_{fmin}^{fmax} \int_{0}^{2\pi} f^n \cdot E(f,\theta)\, d\theta\, df.$
Significant wave height	Hs	$Hs = 4\sqrt{m_o}.$
Mean wave direction	Dir	$\mathrm{Dir} = \mathrm{arctg}\left[\frac{\int \sin\theta \cdot E(f,\theta) df\, d\theta}{\int \cos\theta \cdot E(f,\theta) df\, d\theta}\right].$
Mean zero-crossing period	Tm_{02}	$Tm_{02} = 2\pi\sqrt{\frac{m_0}{m_2}}.$
Peak wave period	Tp	Period corresponding to the maximum energy

interpolation performed by the SWAN model: a spatial interpolation in the discrete components of the spectra; hereafter the integral parameters are computed.

3.2 Yearly analysis

Four different configurations have been tested for a one-year period and validated in three different locations. In these sections only the most representative results are presented. That implies that two unique locations will be shown: the Tarragona deep water buoy, since it is the only one located in the open sea, and the Barcelona coast buoy. The results obtained from the Tarragona coast buoy present very similar behaviour to the Barcelona coast buoy, and the observed differences will be mentioned in the discussion but not shown in detail.

A comparison between the results from the different configurations and the Barcelona coast buoy measurements are represented in the Taylor diagrams in Figure 5 for the significant wave height and the mean wave period, respectively. The results for the peak period are not presented but have behaviour very similar to the Tm_{02}. From the graphics it is straightforward to declare that configurations A and B have almost the same statistics, while configuration C is slightly further from the buoy point and configuration D presents the worst results.

In the first columns of Table 6 the statistic for the significant wave height are shown, with a RMSE around 22 cm and a negative bias of 5 cm in all the configurations except D. The correlation coefficient is very good for configurations A, B and C, with values around .92, but SI is slightly high, around .30. Configuration D is the only one presenting a positive bias.

Also in Table 6 the results for the mean period are presented. The RMSE is around 0.6 s for configurations A, B and C, and the bias is not very important except for configuration D, where a clear overestimation is present. The correlation coefficients take values around .80, and SI has values around .16.

The wave direction is validated with RMSE around 36°, a very low scatter index and a correlation coefficient of .68 in the best situations.

In summary, configurations A, B and C have a similar quality for the significant wave height, while configurations A and B work slightly better than C for the mean period and the wave direction. For the three wave parameters considered, configuration D is clearly the one presenting the worst results, showing an overestimation of the significant wave height and the mean wave period not present in the other alternatives.

Almost the same conclusions may be extracted from the comparison between the four configurations and

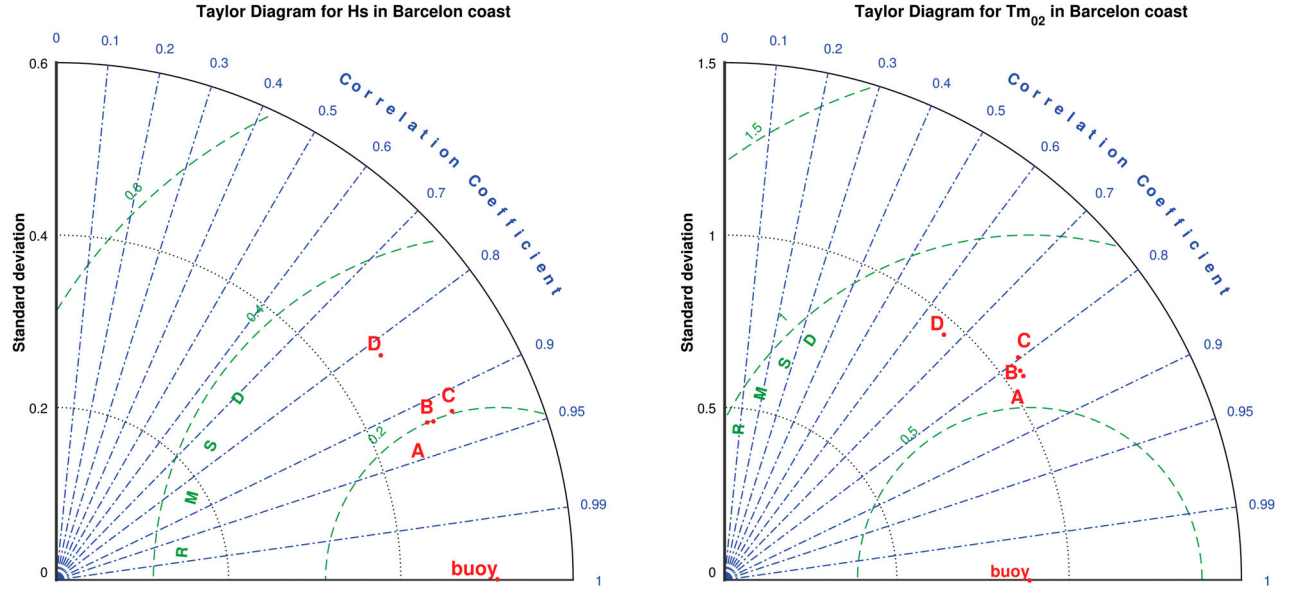

Figure 5. Taylor diagram of the significant wave height (left) and the mean wave period (right) for the annual analyse in the Barcelona coast location. The letters correspond to the configurations tested.

Table 6. Results of the validation of the four configurations including the significant wave height (m), the mean wave period (s) and the wave direction (deg) for the 2013 year in Barcelona coast buoy location.

	Hs				Tm				Dir		
	RMSE [m]	Bias [m]	SI	*R*	RMSE [s]	Bias [s]	SI	*R*	RMSE [°]	SI	*R*
A	0.227	−.053	.304	.921	0.602	.076	.155	.827	33.93	.094	.686
B	0.223	−.048	.299	.922	0.614	.092	.158	.816	33.69	.094	.681
C	0.227	−.046	.304	.920	0.654	.083	.169	.798	36.25	.101	.668
D	0.295	.156	.396	.823	0.849	.726	.219	.668	54.35	.151	.534

the measurements of the Tarragona coast buoy (not shown). The main differences derive from the fact that the mean values of the variables are smaller, so the RMSEs are also smaller, and the correlation coefficients slightly worse (e.g. around .86 for the significant wave height or .68 for the mean period).

The results from the validation process for the deep-water Tarragon buoy are presented in Figure 6, where the Taylor diagrams for the significant wave height and the mean wave period are shown. From the diagrams it can be declared that there are no important differences between configurations A, B and C, while configuration D tends to work slightly worse mainly for the mean wave period.

The results in Table 7 show that, in contrast with the previous case, configuration D does not present results very different from the others for the significant wave height in terms of correlation coefficient. At this point located in deep water the RMSEs are around 25 cm; the bias is negative in all the configurations except D, as was happening in coastal waters; and the correlation coefficients tend to be higher than in coastal zones, between .91 and .94.

Similar behaviour is identified when looking at the mean wave period in Table 7. The RMSE is around 0.60 s, there is an underestimation of the Tm_{02} in all the configurations except D, and the correlation coefficients and scatter index are better than in coastal areas.

The wave direction is analysed in the last columns of Table 7. In deep water the RMSE is slightly higher, around 37°, for configurations A, B and C, while for configuration D the RMSE is smaller than in coastal areas. In general the correlation coefficients are better, with values around .70 for configurations A, B and C, and .6 for configuration D (still better than in coastal areas).

In summary, the four configurations have good accuracy for the significant wave height, but D is the worst among them. For the mean wave period the bad behaviour of configuration D is enhanced. However, in general all the configurations work better in deep water than in coastal areas.

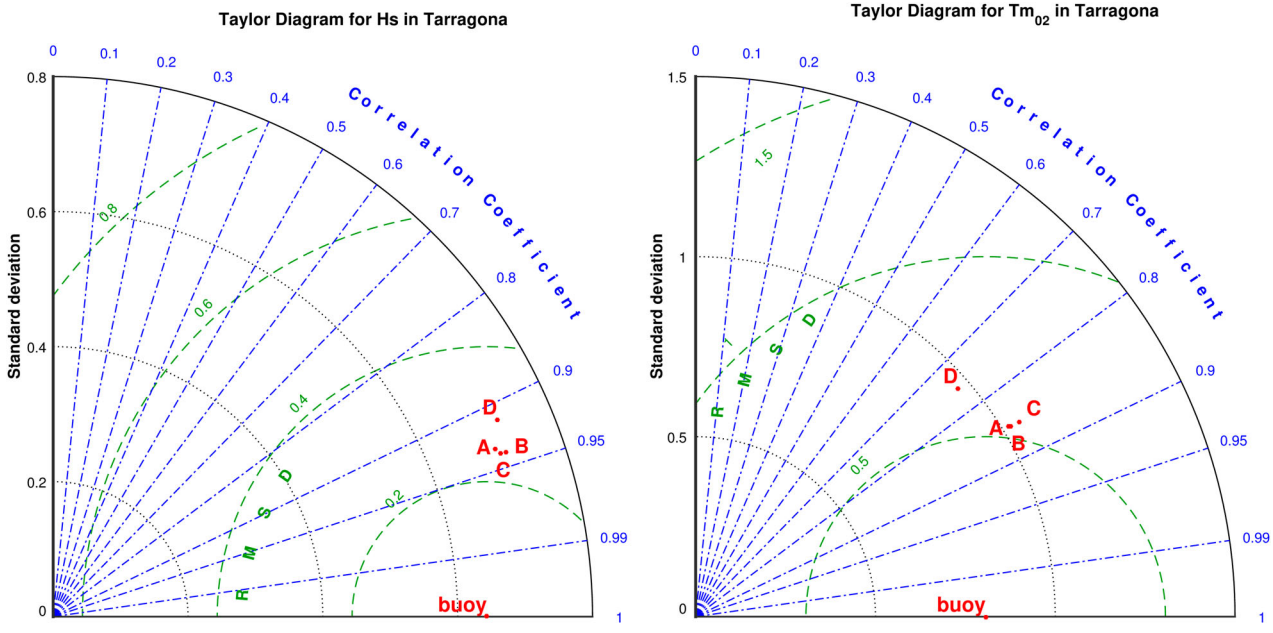

Figure 6. Taylor diagram of the significant wave height (left) and the mean wave period (right) for the annual analyse in the Tarragona location. The letters correspond to the configurations tested.

Table 7. Results of the validation of the four configurations including the significant wave height (m), the mean wave period (s) and the wave direction (deg) for the 2013 year in Tarragona buoy location.

	Hs				Tm				Dir		
	RMSE [m]	Bias [m]	SI	*R*	RMSE [s]	Bias [s]	SI	*R*	RMSE [°]	SI	*R*
A	0.249	−.033	.276	.935	0.614	−.262	.149	.855	37.83	.105	.685
B	0.245	−.025	.271	.940	0.607	−.248	.148	.856	36.89	.103	.714
C	0.242	−.022	.268	.939	0.604	−.210	.147	.857	37.71	.105	.704
D	0.323	.150	.358	.914	0.683	.321	.166	.755	48.43	.135	.606

3.3 Storm analysis

The previous results show the average behaviour of the four configurations over a one-year period. However, one of the main purposes of an operational forecast system is to be able to predict a storm event a few days in advance. For this reason, the annual results have been analysed in order to identify all the storm events reaching the coast. The criteria used to define a storm were a significant wave height threshold of 2 m and a minimum duration of 8 h (Lin-Ye et al. 2016). At the Tarragona deep-water location seven storms were detected, with significant wave heights at the peak of the storm between 3 and 4.5 m. However, only three of them reached the coast and were detected from the Barcelona coast buoy or Tarragona coast buoy. The three storms had a similar pattern, occurring during autumn and winter and generated by important east winds. Since one of them was particularly intense and caused severe damages on the Catalan coast, it has been selected for the present study. The chosen storm occurred between the 26th of February 2013 and the 6th of March 2013, and it presents a two-peak profile. The first peak reaches a significant wave height of 4.5 m, and the second one between 3 and 4 m depending on the locations.

In Figure 7 the time series for the significant wave height, the mean wave period and the direction, both observed and modelled, are presented for the Barcelona coast and Tarragona locations. The storm also reached the Tarragona coast buoy, but the results are not shown due to their similarity to the Barcelona buoy. From a qualitative analysis it seems that the four configurations tested work properly for the first storm peak but present some errors for the second one.

The statistics obtained for the Barcelona coast buoy, presented in Table 8, show that for significant wave height there is almost no differences between configurations A, B and C, while configuration D presents the worst results, with a RMSE that doubles the others. It is interesting to remark that during the storm event configuration D presents an important negative bias in contrast with what is happening in the annual mean, where configuration D presents an overestimation. For the mean wave period, configurations A and B have similar behaviour, while C and D present some problems in the RMSE for the first one and the correlation coefficient in the second one. The bias for all the configurations is higher than that observed for the annual average. The direction is quite constant during the entire event and is well represented by the four configurations, although A and B present better results than C and D.

The results in deep waters, presented in Table 9, show that, in contrast with the results for coastal areas, the significant wave height has better behaviour for configurations A and B than for configurations C and D, which depend on the boundary conditions obtained from the operational model. As previously seen, configuration D tends to underestimate the significant wave height during storm events as opposed to the annual behaviour. For the mean wave period and the mean wave direction similar observations can be made.

In conclusion, configurations A and B work best, and configuration D is the one presenting the worst results. The main difference can be found in configuration C, which works fine in coastal areas but not so well in deep waters.

3.4 Computational time requirements

Until now the comparison has been focused on the accuracy and quality of the results. However, there is another key point to account for in the comparison: the computational time required to obtain the results. This aspect can become vital in an early warning system when the information is required as soon as possible in order to be able to take decisions.

Following this idea, a comparison of the four configurations described in Section 2.4 has been carried out. The selected period for the comparison was June 2013, and the computer used is the one described in Section 2.6.

The results for each of the grids are presented in the third column of Table 10. The total time for each configuration can be obtained as the sum of the time required for each of the domains included in it. When necessary, the time required to extract the boundary conditions from the actual operational system and transform it to introduce them in SWAN is included. The results show a reduction of time of about 66% from the traditional way of providing a high-resolution wave forecast

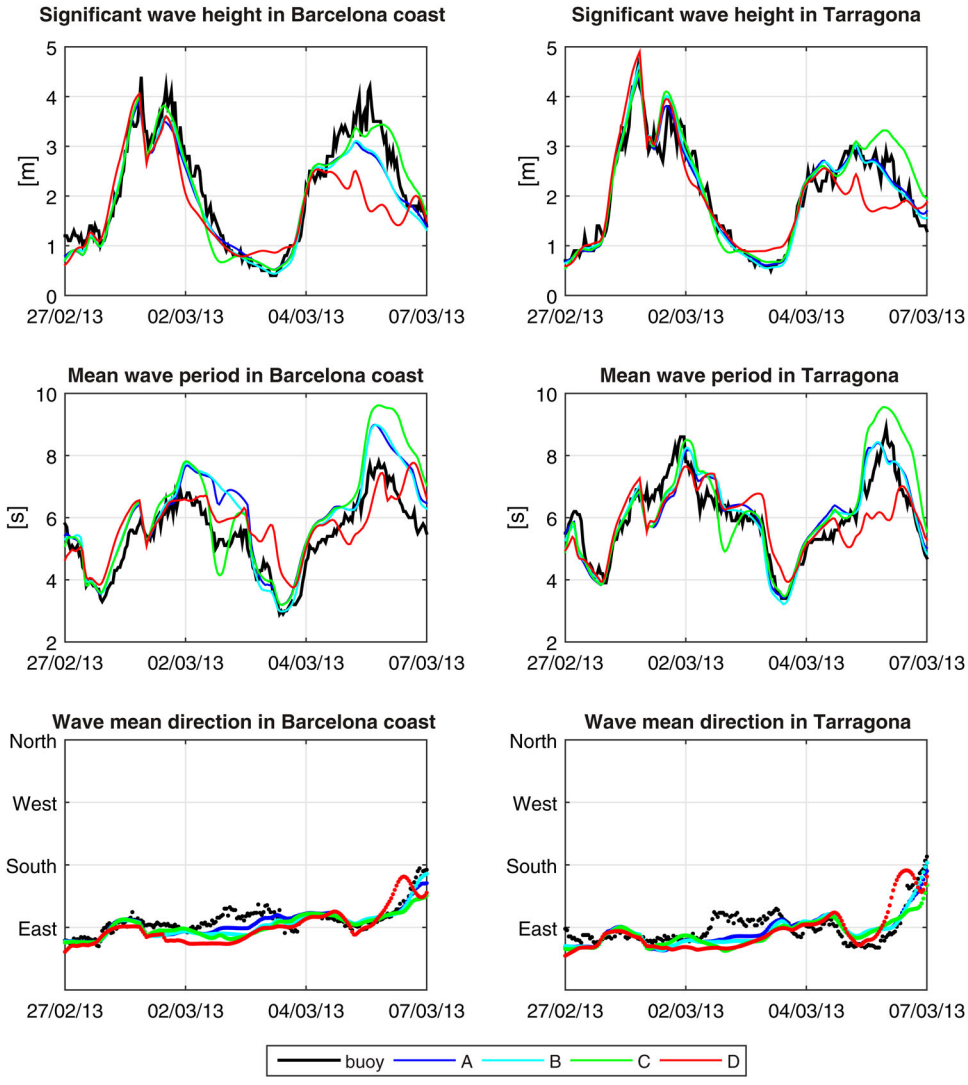

Figure 7. Time series for the significant wave height (first row), the mean wave period (second row) and the mean wave direction (third row) for the Barcelona coast location (first column) and the Tarragona location (right column) during the storm event. In black the buoy measurements are represented, while the colours correspond to the four configurations tested.

Table 8. Results of the validation of the four configurations including the significant wave height (m), the mean wave period (s) and the wave direction (deg) for the storm event in Barcelona coast buoy location.

	Hs				Tm				Dir		
	RMSE [m]	Bias [m]	SI	*R*	RMSE [s]	Bias [s]	SI	*R*	RMSE [°]	SI	*R*
A	0.364	−.190	.171	.965	0.871	.656	.162	.935	11.31	.031	.943
B	0.351	−.209	.165	.969	0.860	.611	.160	.940	13.45	.037	.811
C	0.326	−.068	.153	.958	1.049	.693	.196	.925	16.29	.045	.689
D	0.689	−.301	.324	.826	0.808	.394	.151	.796	20.81	.058	.676

Table 9. Results of the validation of the four configurations including the significant wave height (m), the mean wave period (s) and the wave direction (deg) for the storm event in Tarragona buoy location.

	Hs				Tm				Dir		
	RMSE [m]	Bias [m]	SI	*R*	RMSE [s]	Bias [s]	SI	*R*	RMSE [°]	SI	*R*
A	0.222	.008	.108	.975	0.565	.045	.094	.899	16.19	.045	.754
B	0.233	.005	.113	.975	0.532	.010	.088	.915	17.64	.049	.722
C	0.370	.137	.180	.949	0.809	.227	.134	.873	21.53	.060	.546
D	0.438	−.058	.213	.903	0.822	−.130	.136	.756	24.60	.068	.608

Table 10. Computational time requirements for each of the grids used in the study (third column) and for each configuration tested (fourth column).

Configuration	Grids used	Grid time	Total time
A	Mediterranean regular	7 h 46 min	24 h 17 min
	Balear regular	8 h 10 min	
	Local regular	8 h 21 min	
B	Mediterranean unstructured	8 h 11 min	8 h11 min
C	Processing boundary conditions	10 min	17 h 32 min
	Balear regular	9 h 1 min	
	Local regular	8 h 21 min	
D	Processing boundary conditions	10 min	14 h 43 min
	Balear unstructured	14 h 33 min	

(the nested grids, configuration A) to the regional unstructured grid proposed in the present study (configuration B). Configuration C, using boundary conditions from an operational system, presents a reduction of time of about 23% with respect to configuration A. Finally, the Balear unstructured grid (configuration D) is faster than configuration C but slower than configuration B due to the time required to read the boundary conditions, despite configuration D having fewer nodes than B.

4. Discussion

In the present study the use of unstructured grids is presented as an alternative to the traditional downscaling methods consisting of a series of nested grids. The unstructured grids (Figure 2) allow the boundary conditions to be removed, obtaining high-resolution forecasts in less computational time. However, it should be taken into account that designing an efficient unstructured grid is a long process, and still some small problems can appear, as happens with configuration D (Pallares 2016).

From the analysis of annual results it can be concluded that using a system of nested grids (configuration A) or a regional unstructured grid (configuration B) provides almost the same results, so there is no effect of the meshes used on the accuracy of the forecast. Some differences may appear when nesting the local grids (regular as in configuration C or unstructured as in configuration D) due to the boundary conditions. These differences mainly depend on the quality of the boundary conditions for regular grids. From the present study it can be stated that using good boundary conditions generates forecasts very similar to the ones generated by a regional model.

The mentioned differences are more relevant when nesting an unstructured grid into a regular regional system (configuration D), obtaining lower correlation coefficients and presenting a slight overestimation of the results not seen in the other configurations. It should be pointed out that in the SWAN model it is possible to introduce boundary conditions in two different ways: providing the full spectrum in all the boundary points, or providing some bulk parameters (significant wave height, wave period, wave direction and wave spread) and letting the model calculate a theoretical spectrum with this information. In both configurations C and D, the second option has been used, but only some problems have been detected with the unstructured grid (configuration D). In order to assure that the small problems in configuration D are due to the reading of the boundary conditions and not related to the grid design, some additional tests have been carried out. When running configuration D using the full spectra as boundary conditions, obtained directly from SWAN simulations in the biggest grid of configuration A, the obtained results are almost equivalent to the ones from configuration C. From the analysis of the test it seems that the local unstructured grid only works properly when the boundary conditions are provided as a spectra (not always available from an operational forecast service), and some errors appear when the boundary conditions are provided in parameter form.

A storm event has also been analysed, with very similar conclusions. Although during energetic events the different configurations tend to work better than for the annual average, the behaviours of the different configurations are very similar. The regional configurations (A and B) present very similar results, confirming that there is almost no contrast between unstructured grids and regular nested grids. The differences, more important during energetic events, appear when introducing boundary conditions from an operational forecasting system.

The computational time required is the key point of the configuration comparison. All the considered configurations present a reduction of time with respect to the traditional methodology, with the unstructured regional grid being the most important, with a decrease of around 66% without losing quality in the wave forecast. The local regular domains nested in a forecast system also present very good results and a reduction of time of 23% with respect to the traditional methodology.

The unstructured grids have considerably fewer points than the regular grids (Table 1). However, the numerical scheme for these grids is slower, obtaining a total computational time per grid of the same order of magnitude as a regular grid. The advantage derives from the fact that only one unstructured grid is necessary as compared to a system of several nested grids.

One last critical point is that the Mediterranean unstructured grid is faster than the Balear unstructured grid despite having a greater number of nodes. This increase of time is due to the process of reading and interpolating the boundary conditions from several

locations at the boundaries into the grid nodes located at the boundaries (not regularly distributed). When working with boundary conditions in spectral form, the time required to run the Balear unstructured grid is reduced to 5 h and 12 min.

5. Conclusions

In recent years the application of unstructured grids in wave modelling has been gaining relevance. In the present study an unstructured grid applied to a regional environment like a semi-enclosed sea is compared to the traditional downscaling method in terms of both the accuracy of the results and the computational time required. Two local grids (one regular and the other unstructured) nested in an operational system are also included in the comparison. The main conclusions obtained are the following:

- Designing a good unstructured grid is a hard process that only needs to be done once. After obtaining an efficient and accurate unstructured grid, it is possible to achieve the same forecast accuracy and costal resolution as the traditional downscaling method, with an important reduction of the computational time.
- For semi-enclosed domains it is more interesting to generate a regional unstructured grid than a local grid nested into an operational forecasting system. However, if the operational system provides good boundary conditions, as happens in the present study, the local nested grid may provide accurate results with a reduction of time with respect to the traditional method.
- The SWAN model may present some differences when using boundary conditions in parameter format in unstructured grids with respect to regular grids. These differences disappear when the boundary conditions come in a spectral format.

Acknowledgements

The authors want to acknowledge the Spanish meteorological agency (Agencia Estatal de Meteorologia, AEMET, Ministerio de Agricutura, Alimentación y Medio Ambiente) for providing the wind fields for the present study, the Spanish harbour authority Puertos del Estado for providing the buoy measurements data and boundary conditions, and the Secretaria d'Universitats i Recerca del Dpt. d'Economia i Coneixement de la Generalitat de Catalunya (ref. 2014SGR1253).

Disclosure Statement

No potential conflict of interest was reported by the authors.

Funding

This work has been performed in the framework of the Spanish national project PLANWAVE (ref. CTM2013-45141-R) from the MINECO and FEDER and the European project iCOAST (no. ECHO/SUB/2013/661009) funded by the European Commission, Directorate – General Humanitarian Aid and Civil Protection – ECHO, A.5 Civil Protection Policy, Prevention, Preparedness and Disaster Risk Reduction Unit.

ORCID

Elena Pallares http://orcid.org/0000-0003-2656-2311
Manuel Espino http://orcid.org/0000-0002-9026-3976
Agustín Sánchez-Arcilla http://orcid.org/0000-0002-3450-6697

References

Alari V, Raudsepp U, Kouts T. 2008. Wind wave measurements and modelling in Küdema bay, Estonian Archipelago sea. J Mar Res. 74:S30–S40.

Alomar M, Sanchez-Arcilla A, Bolaños R, Sairouni A. 2014. Wave growth and forecasting in variable, semi-enclosed domains. Cont Shelf Res. 87:28–40.

Ardhuin F, Bertotti L, Bidlot J, Cavaleri L, Filipetto V, Lefevre J, Wittmann P. 2007. Comparison of wind and wave measurements and models in the western Mediterranean sea. Ocean Eng. 34:526–541.

Arnau PA. 2000. Aspectos de la variabilidad de mesoescala de la circulación marina en la plataforma continental catalana [PhD thesis]. Barcelona: Universitat Politecnica de Catalunya.

Bolaños R, Jordà G, Cateura J, Lopez J, Puigdefabregas J, Gomez J, Espino M. 2009. The XIOM: 20 years of a regional coastal observatory in the Spanish Catalan coast. J Mar Res. 77:237–260.

Bolaños R, Sánchez-Arcilla A, Cateura J. 2007. Evaluation of two atmospheric models for wind-wave modelling in the NW Mediterranean. J Mar Res. 65:336–353.

Booij N, Ris R, Holthuijsen L. 1999. A third-generation wave model for coastal regions: 1. Model description and validation. J Geophys Res. 104:7649–7666.

Cavaleri L, Malanotte-Rizzoli P. 1981. Wind wave prediction in shallow water: theory and applications. J Geophys Res. 86:961–973.

Gomez Lahoz M, Carretero Albiach J. 2005. Wave forecasting at the Spanish coasts. J Atmos Ocean Technol Sci. 10:389–405.

Gracia V, García-Leon M, Sánchez-Arcilla A, Gault J, Oller P, Fernández J, Sairouni A, Cristofori E, Toldrà R. 2014. A new generation of early warning system for coastal risk. The iCoast project. International Conference in Coastal Engineering, ICCE 2014, Seoul, Korea.

Hasselmann K, Hasselmann K, Allender JH, Barnett TP. 1985. Computations and parameterizations of the nonlinear energy transfer in a gravity-wave specturm. Part II: parameterizations of the nonlinear energy transfer for application in wave models. J Phys Oceanogr. 15:1378–1391.

Hsu T, Ou S, Liau J. 2005. Hindcasting nearshore wind waves using a FEM code for SWAN. Coast Eng. 52:177–195.

Komen GJ, Hasselmann S, Hasselmann K. 1984. On the existence of a fully developed wind-sea spectrum. J Phys Oceanogr. 14:1271–1285.

Lin-Ye J, Garcia-Leon M, Gracia V, Sanchez-Arcilla A. Forthcoming 2016. A multivariate model of NW Mediterranean extreme events: hydrodynamics, energy and duration. Coast Eng.

Pallares E. 2016. High-resolution wave forecasting. The Catalan coast case. Modelling, coupling and validation [Ph.D. thesis]. Barcelona: Universitat Politecnica de Catalunya.

Pallares E, Sánchez-Arcilla A, Espino M. 2014. Wave energy balance in wave models (SWAN) for semi-enclosed domains – application to the Catalan coast. Cont Shelf Res 87:41–53.

Ris R, Holthuijsen L, Booij N. 1999. A third-generation wave model for coastal regions: 2. Verification. J Geophys Res. 104:7667–7681.

Sánchez-Arcilla A, González-Marco D, Bolaños R. 2008. A review of wave climate and prediction along the Spanish Mediterranean coast. Nat Hazards Earth Syst Sci. 8:1217–1228.

Sánchez-Arcilla A, Wolf J, Monbaliu J. 2014. Oceanography at coastal scales: introduction to the special issue on results from the EU FP7 FIELD_AC project. Cont Shelf Res. 87:1–6.

Siadatmousavi S, Jose F, Miot da Silva G. 2015. Sensitivity of a third generation wave model to wind and boundary condition sources and model physics: a case study from the south Atlantic Ocean off Brazil coast. Comput Geosci. 90:57–65.

Snyder RL, Dobson FW, Elliott JA, Long RB. 1981. Array measurements of atmospheric pressure fluctuations above surface gravity waves. J. Fluid Mech. 102:1–59.

SWAN team. 2015a. SWAN user's manual. SWAN Cycle III version 40.91A. Delft University of Technology. Technical documentation.

SWAN team. 2015b. SWAN scientific and technical documentation. SWAN Cycle III version 40.91A. Delft University of Technology. Technical documentation.

Taylor K. 2001. Summarizing multiple aspects of model performance in a single diagram. J Geophys Res Atmos. 106:7183–7192.

Unden P, Rontu L, Jarrinen H, Lynch P, Calvo J, Cats G, Cuxart J, Eerola K, Fortelius C, Garcia-Moya JA, et al. 2002. HIRLAM-5 scientific documentation. Available from: www.hirlam.org

WAMDI group. 1988. The WAM model – a third generation ocean wave prediction model. J Phys Oceanogr. 18:1775–1810.

Zijlema M. 2010. Computation of wind-wave spectra in coastal waters with SWAN on unstructured grids. Coast Eng. 57:267–277.